



# Biogenic Synthesis of MnO<sub>2</sub> Nanoparticles With Leaf Extract of *Viola betonicifolia* for Enhanced Antioxidant, Antimicrobial, Cytotoxic, and Biocompatible Applications

Haibin Lu<sup>1,2</sup>, Xueyang Zhang<sup>1,2</sup>, Shakeel Ahmad Khan<sup>3</sup>, Wenqiang Li<sup>4\*</sup> and Lei Wan<sup>2\*</sup>

<sup>1</sup>Shunde Hospital, Southern Medical University (The First People's Hospital of Shunde), Foshan, China, <sup>2</sup>Stomatological Hospital, Southern Medical University, Guangzhou, China, <sup>3</sup>Center of Super-Diamond and Advanced Films (COSDAF), Department of Chemistry, City University of Hong Kong, Kowloon, Hong Kong, <sup>4</sup>Engineering Technology Research Centre for Sports Assistive Devices of Guangdong, Guangzhou Sport University, Guangzhou, China

## OPEN ACCESS

### Edited by:

Dmitry Skladnev,  
Russian Academy of Sciences,  
Russia

### Reviewed by:

Hayssam M. Ali,  
King Saud University, Saudi Arabia  
Karthik Loganathan,  
Salem Microbes Pvt Ltd, India

### \*Correspondence:

Wenqiang Li  
gztylwq@foxmail.com  
Lei Wan  
wanleilucky@126.com

### Specialty section:

This article was submitted to  
Microbiological Chemistry and  
Geomicrobiology,  
a section of the journal  
Frontiers in Microbiology

**Received:** 19 August 2021

**Accepted:** 11 October 2021

**Published:** 01 November 2021

### Citation:

Lu H, Zhang X, Khan SA, Li W and  
Wan L (2021) Biogenic Synthesis of  
MnO<sub>2</sub> Nanoparticles With Leaf  
Extract of *Viola betonicifolia* for  
Enhanced Antioxidant, Antimicrobial,  
Cytotoxic, and Biocompatible  
Applications.  
Front. Microbiol. 12:761084.  
doi: 10.3389/fmicb.2021.761084

In this study, we propose to synthesize NPs using plant extract containing active biomedical components, with the goal of obtaining NPs that inherit the biomedical activities of the plant. Herein, we report the synthesis of manganese dioxide nanoparticles (VBLE-MnO<sub>2</sub> NPs) using the leaves extract of *Viola betonicifolia*, in which the biological active plant's secondary metabolites function as both reducing and capping agents. The synthesized NPs were successfully characterized with different spectroscopic techniques. The antibacterial, antifungal, and biofilm inhibition properties of the synthesized VBLE-MnO<sub>2</sub> NPs were further explored against a variety of bacteria (Gram-positive and Gram-negative) and mycological species. Additionally, their antioxidant ability against linoleic acid peroxidation inhibition, cytobiocompatibility with hMSC cells, and cytotoxicity against MCF-7 cells were investigated compared to leaves extract and chemically synthesized manganese dioxide NPs (CH-MnO<sub>2</sub> NPs). The results were demonstrated that the synthesized VBLE-MnO<sub>2</sub> NPs presented excellent antibacterial, antifungal, and biofilm inhibition performance against all the tested microbial species compared to plant leaves extract and CH-MnO<sub>2</sub> NPs. Moreover, they also exhibited significant antioxidant potential, which was comparable to the external standard (ascorbic acid); however, it was higher than plant leaves extract and CH-MnO<sub>2</sub> NPs. Furthermore, the synthesized CH-MnO<sub>2</sub> NPs displayed good cytobiocompatibility with hMSC cells compared to CH-MnO<sub>2</sub> NPs. The enhanced antioxidant, antibacterial, antifungal, and biofilm inhibition efficacy as compared to CH-MnO<sub>2</sub> NPs might be attributed to the synergistic effect of the VBLE-MnO<sub>2</sub> NPs' physical properties and the adsorbed biologically active phytochemicals from the leaves extract of *V. betonicifolia* on their surface. Thus, our study establishes a novel ecologically acceptable route for nanomaterials' fabrication with increased and/or extra medicinal functions derived from their herbal origins.

**Keywords:** MnO<sub>2</sub> NPs, antimicrobial, biofilm inhibition, antioxidant, cytotoxic

## INTRODUCTION

Antibiotic and antifungal drug resistance in pathogenic bacterial and fungal species have emerged as an alarming threat globally (Khan et al., 2020a). A significant reason behind the antimicrobial drugs not working is the formation of biofilms by these microbials (Khan et al., 2021c). These pathogenic microbials in biofilms form can withstand a thousand dosages of conventional antimicrobial medicines (Khan and Lee, 2020b). Moreover, these pathogenic microbials have also evolved resistance to antimicrobial drugs by developing efflux mechanisms, decreasing the cell wall permeation, modifying the drug targeted sites, etc. (Li and Nikaido, 2009; Khan et al., 2020b). Therefore, these antimicrobial drugs are failing to treat different infectious diseases caused by these pathogenic microbial species. The current death burden due to infectious disease caused by pathogenic microbials is around 0.7 million deaths annually, as per World Health Organization. This can be risen to approximately 10 million annually by 2050 if effective and novel antimicrobial agents are not developed (Khan et al., 2020a; New report calls for urgent action to avert antimicrobial resistance crisis, 2021). In this instance, nanotechnology has emerged and come to the forefront to confront antimicrobial resistance issues by developing nanosized materials.

NPs, among other nanomaterials, are attracting so much attention worldwide because of their unique physical characteristics. Moreover, NPs present excellent biological, electrical, sensing, and optoelectronics applications due to their physical characteristics. National Nanotechnology Initiative has spent more than 27 billion dollars in the United States during the last 10 years. Moreover, the European Commission has initiated HORIZON 2020 projects in the nanotechnology sector with around €1.1 billion. In Asia, China and Japan are investing vast amounts of resources and funds for nanoscience and nanotechnology, which resulted in prices rising by 20 percent nearly every year since 2003 (Ciorîță et al., 2020; Home National Nanotechnology Initiative 2021). Metals (Au, Ag, Pt, Pd, Mn, Zn, Cu, etc.) and metal oxides (CuO, MnO, ZnO, NiO, MgO, FeO, Fe<sub>2</sub>O<sub>3</sub>, Cr<sub>2</sub>O<sub>3</sub>, etc.) NPs are widely exploited and investigated for different biological application, such as antibacterial, antimycotic, antibiofilm, antioxidant, and anticancer (Abbasi et al., 2019a,b; Al-Radadi, 2019; Haq et al., 2020; Khan et al., 2020a,b, 2021b; Khan and Lee, 2020a). In contrast to traditional antibacterial and antifungal medicines, these NPs readily penetrate pathogenic microorganisms' cell walls and membranes due to their nanoscale size. This is a key element in the antimicrobial activities of these NPs (Khan et al., 2020a). Furthermore, MnO<sub>2</sub> NPs have been much attracted due to their low potential cytotoxicity compared to others.

Generally, NPs are produced through chemical or physical methods. However, both approaches need significant amounts of energy and hazardous chemicals for reduction and capping, and they are not readily scalable (Ciorîță et al., 2020; Khan et al., 2020a,b). A critical issue is that these methods jeopardize the biocompatibility of NPs owing to using dangerous chemicals in the manufacturing process, which remain on the NPs' interface also after repeated washing. As a result, their biological

applicability is jeopardized (Negahdary et al., 2015; Ogunyemi et al., 2019; Ciorîță et al., 2020). Thus, the synthesis of NPs utilizing biological approaches, particularly those based on plants, offers a solution to these established methodologies (Ciorîță et al., 2020; Khan et al., 2020a,b). It has been shown that the phytochemical constituents present in plants, including, alkaloids, polyphenols, flavonoids, and terpenoids, induce the reduction of metal ions and eventual formation of metal NPs (Elbagory et al., 2019; Gharehyakheh et al., 2020). Moreover, it is considered that biogenic plant phytochemicals may enhance their intrinsic properties, such as antioxidant, antibacterial, and anticancer compared to extracts (Chandran et al., 2006; Kumar and Yadav, 2009; Muthukumar et al., 2016). Thus, biogenic synthesis using leaves extract of plants enhances the nanoparticle biocompatibility and is responsible for the synergetic effect (Khan and Lee, 2020a).

In this regard, leaves extract of *Viola betonicifolia* (L.), a species of family *Violaceae*, was used for bioconversion of manganese ions to NPs. *V. betonicifolia* (L.) is naturally available in several countries over the globe, including Pakistan, India, Nepal, Sri Lanka, China, Malaysia, Burma, and Australia (Flora of Pakistan; Rizwan et al., 2019). This plant has been widely exploited as purgative, astringent, diaphoretic, anticancer, antipyretic, and employed for treating various diseases, such as nervous disorders, epilepsy, cough, skin disorders, blood disorders, sinusitis, pharyngitis kidney diseases, bronchitis, and pneumonia (Iqbal and Hamayun, 2005; Rizwan et al., 2019). Various reports demonstrated that the whole leaves extract of *V. betonicifolia* is a rich source of several biogenic phytochemicals, including alkaloids, flavonoids, tannins, phenolic compounds, saponins, and triterpenoids with various biological applications (Muhammad et al., 2012, 2013a). Almost 200 natural active compounds have been identified and isolated from various *Viola* species (Zhu et al., 2015). Up to now, many plants have been utilized for the biogenic synthesis of MnO<sub>2</sub> NPs; however, there is no report for the utilization of *V. betonicifolia* (L.). Therefore, here for the first time, we report the biogenic synthesis of MnO<sub>2</sub> NPs using *V. betonicifolia* (L.) leaves extract. Further considering the leaf leaves extract of *V. betonicifolia* health benefits in the biomedical field, herein, biologically synthesized MnO<sub>2</sub> NPs were evaluated for antimicrobial, anticancer, and antioxidant activities.

## MATERIALS AND METHODS

All the chemicals used in this work were purchased from Sigma Chemicals Co (St, Louis, MS, United States) and Merck (Darmstadt Germany) and were analytical grade. The commercially available MnO<sub>2</sub> NPs were purchased from US Research Nanomaterials, Inc. with 30–50 nm size for comparative biological analysis. These NPs are called as CH-MnO<sub>2</sub> NPs.

### Collection of the Plant Material

The fresh *V. betonicifolia* leaves were collected from the surrounding areas of Lahore, Pakistan. Dr. Zaheer-ud-Din

Khan (Department of Botany, GC University, Pakistan) made its identification. The voucher specimen (*V. betonicifolia*: GC. Herb. Bot. 213) of plant was deposited at the herbarium of the Department of Botany, GC University, Lahore, Pakistan, and further study approval is not required as per regional guidelines.

## Preparation of Leaves Extract of *Viola betonicifolia*

The leaves extract of *V. betonicifolia* was prepared by taking 20 g of fresh leaves of *V. betonicifolia*. The leaves were washed thoroughly with deionized (DI) water to remove any impurities and dust and air-dried at 30°C. The dried leaves were cut into small pieces, pulverized with the help of a commercial blender, and the resulting plant's leaves powder was transferred to a 500 ml beaker. The 150 ml of DI water was then added and stirred at 60°C for 60 min. After, the obtained leaves extract of *V. betonicifolia* was cooled down to room temperature and then filtered. The filtrate was collected and stored at 4°C in an airtight glass bottle for further use (Figure 1).

## Biogenic Synthesis of Manganese Dioxide NPs (VBLE-MnO<sub>2</sub> NPs)

For the biogenic synthesis of manganese dioxide NPs, 1 mm of Manganese acetate was added to 25 ml of leaves extract of *V. betonicifolia* (Figure 1). The resulting mixture was heated at 40°C for 70 min with continuous stirring at pH 7.15. After, the synthesized manganese dioxide NPs were separated by centrifugation at 3000 rpm for 30 min from the reaction mixture. After centrifugation, the obtained NPs were washed with DI/ethanol three times and then dried in an oven at 40°C and

further calcined in a muffle furnace at 200°C for 3 h. Finally, the green synthesized manganese dioxide NPs were stored in a glass bottle for further characterization and named as VBLE-MnO<sub>2</sub> NPs.

## Characterization

### X-ray Diffraction

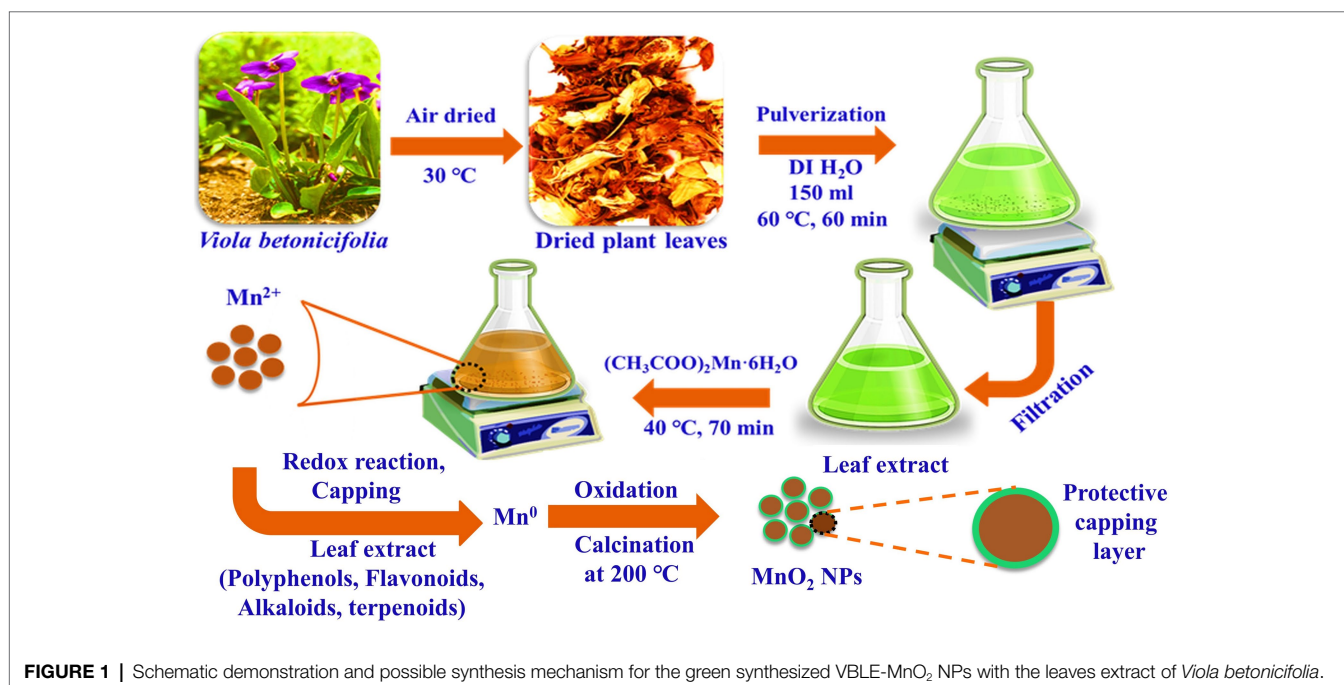
The crystalline nature and phase purity of the green synthesized VBLE-MnO<sub>2</sub> NPs were determined using the powder X-ray diffraction spectroscopy (XRD), which was carried out at a wavelength ( $\lambda$ ) of 0.154 nm with LYNXEYE XE-T detector (Haidian, Beijing, China) in a Bruker D2 PHASER. The XRD spectra were recorded in the  $2\theta$  range 20–60°, with a scanning rate of 1°/min and a slit width of 6.0 mm.

### Energy-Dispersive X-ray Spectroscopy

The chemical composition of synthesized VBLE-MnO<sub>2</sub> NPs was performed with an energy-dispersive X-ray (EDX) spectroscopy and Thermo Fisher Scientific Ultradry (Madison, WI, United States) which was attached with SEM.

### Transmission Electron Microscope

Transmission electron microscopy (TEM) images of the green synthesized VBLE-MnO<sub>2</sub> NPs were obtained using a Tecnai F12 microscope (FEI/Philips Tecnai 12 BioTWIN, Baltimore, MD, United States) operating at an acceleration voltage of 200 kV (Devi et al., 2019; Khan et al., 2021b). For TEM analysis, the samples were mixed in methanol and then sonicated at 25–30°C. Then, specimens were deposited into a carbon-coated copper grid. After removing the excess solution, the copper grid was left to dry for 5–10 min.



## Zetasizer Dynamic Light Scattering

The stability and the particle size distribution of the fabricated VBLE-MnO<sub>2</sub> NPs were measured at 25–30°C, with a particle size analyzer (Malvern Zetasizer Nano ZS, Worcestershire, WR14 1XZ, United Kingdom; Devi et al., 2019; Khan et al., 2021b).

## Antibacterial Propensity

The antibacterial propensity of the synthesized VBLE-MnO<sub>2</sub> NPs was evaluated on *Klebsiella pneumoniae* ATCC®700603™ and *Staphylococcus aureus* ATCC®23235™, by using serial dilution method (Khan et al., 2021a). In general, the strains of bacteria were seeded into separate blood agar plates and then cultured for 24 h at 37°C. After several bacterium colonies were grown on the plates, they were diluted with phosphate buffer saline (PBS). Their cell density was maintained to 1 × 10<sup>8</sup> colony forming units (CFU) per ml. Following that, 10 μl of each bacterial culture was separately added to wells of a 24-well microtiter plate with 1.0 ml of Mueller-Hinton broth (MHB). For each well, the final concentration of each bacterium was 1 × 10<sup>6</sup> CFU/ml. A 50 μl of each sample solution at 250 μg/ml concentration was then transferred to separate wells and incubated at 37°C for 24 h. The bacterial species were then counted in the wells using the serial dilution plate counting method. The antibacterial propensity was expressed in the form of log<sub>10</sub> reduction in bacterial growth and % killing using the following formulas:

$$\log_{10} \text{reduction} = \log_{10}(\text{CFU}_B) - \log_{10}(\text{CFU}_A)$$

$$\% \text{killing} = (\text{CFU}_B - \text{CFU}_A) / \text{CFU}_B \times 100$$

here, CFU<sub>B</sub> and CFU<sub>A</sub> are the CFU of bacterial strains before and after 24 h of incubation, respectively, with the treatment of sample solutions.

## Live/Dead Bacteria Staining Assay

Live and dead bacterial staining assay was carried out using a confocal laser scanning microscope (CLSM, FV-1200, Olympus, Tokyo, Japan) to confirm the antibacterial activity of green synthesized VBLE-MnO<sub>2</sub> NPs. The assay was performed following the methods reported by Choi et al. (2017). Briefly, two nucleic dyes, Hoechst 33342 (membrane-permeant) and propidium iodide (PI; membrane-impermeant), were used for staining the live (green) and dead (red) bacteria, respectively. Each bacterium was cultured in nutrient broth in an orbital shaker for 24 h at 37°C to reach the stationary phase, which consists of approximately 10<sup>5</sup>–10<sup>6</sup> colony forming units (CFU) per ml. After incubation, each bacteria strain was inoculated into sterilized cover glass coated with poly-L-lysine in a 24-well plate and then incubated for 1 h for bacterial cells attached to the cover glass. The suspended bacterial cells were then discarded, and each cover glass was gently rinsed three times with a saline solution. For the treatment, each bacterium cells on the cover glass were incubated with green synthesized VBLE-MnO<sub>2</sub> NPs (250 μg/ml) and then incubated for 24 h at

37°C. Bacteria cells on cover glass were then stained with an alive and dead bacterial viability kit in accordance with the manufacturer's recommendations. Dead and live bacterial cells were analyzed with CLSM using an excitation wavelength of 493 nm and 350 for PI and Hoechst 33342 and an emission wavelength of 636 nm and 461 nm for PI and Hoechst 33342, respectively. We only considered green synthesized VBLE-MnO<sub>2</sub> NPs for live/dead staining assay as they presented excellent antibacterial properties in terms of Log<sub>10</sub> reductions.

## ROS Generation Investigation in the Nanoparticles-Treated Bacteria

The CellROX®Green staining was further used to examine the death of bacterial species caused by intracellular ROS production. In brief, bacterial species (*K. pneumoniae* and *S. aureus*) at 1 × 10<sup>7</sup> CFU/ml with 70 μl of produced VBLE-MnO<sub>2</sub> NPs at a concentration of 250 μg/ml and incubating at 37°C for 24 h. Following that, the microbial cells were treated for an additional 30 min at 37°C with CellROX®Green (5 μm). Following that, CLSM was utilized to acquire CLSM images at 485 nm absorption and 520 nm emission wavelengths. To assess microbial cells' ability to generate reactive oxygen species (ROS), the results of cells treated with NPs were compared to those treated with 1 mM H<sub>2</sub>O<sub>2</sub> (positive control) and untreated cells (negative control).

## Antifungal Activity

The antifungal activity of the green synthesized VBLE-MnO<sub>2</sub> NPs was estimated on three mycological species, which include *A. fumigatus* (ATCC®13073™), *Trichoderma harzianum* (ATCC®32086™), and *A. flavus* (ATCC®9643™). A same antibacterial activity method as stated before in section 3.5 was performed, but seeding was performed using a Sabouraud-gentamicin-chloramphenicol (SGC) fungus agar plate and the incubation temperature was maintained at 30°C. The antifungal activity was expressed in the form of log<sub>10</sub> reduction in bacterial growth and % killing using the following formulas:

$$\log_{10} \text{reduction} = \log_{10}(\text{CFU}_B) - \log_{10}(\text{CFU}_A)$$

$$\% \text{killing} = (\text{CFU}_B - \text{CFU}_A) / \text{CFU}_B \times 100$$

here, CFU<sub>B</sub> and CFU<sub>A</sub> are the CFU of mycological strains before and after 24 h of incubation, respectively, with the treatment of sample solutions.

## Anticancer Activity

The anticancer activity of the green synthesized VBLE-MnO<sub>2</sub> NPs was determined against the MCF-7 breast cancer cells following the MTT [3-(4,5-dimethylthiazol-2-yl)-2,5-diphenyltetrazolium bromide] colorimetric protocol. The MCF-7 cancer cells were kept in Dulbecco's Modified Eagle's Medium (DMEM) in an incubator which was set at 5% CO<sub>2</sub>, 95% air, and 37°C. To obtain cell confluency up to 5 × 10<sup>8</sup> cells/well, the MCF-7 cells were grown for 24 h at 37°C in 100 μl of

DMEM in a 96-well plate. After 50 µl of VBLE-MnO<sub>2</sub> NPs, plant extract and CH-MnO<sub>2</sub> NPs at a concentration of 1, 10, 20, 40, 60, 80, 100, and 120 µg/ml were added in each well separately containing cultured MCF-7 cells, and the plate was further incubated for 24 h at 37°C. The plate was then centrifuged to remove the supernatant and rinsed with PBS solution. A total of 15 µl of MTT labeling agent (0.5 mg/ml) was then poured into each well; the plate was then put in an incubator for 4 h at 37°C. 150 µl of DMSO was added to each well to solubilize the undissolved crystals of formazan. The absorption maxima of formazan product in each well were measured at 570 nm using a Varian Eclipse spectrophotometer. The percentage of cell viability was calculated using the following formula with the help of the following equation:

$$\% \text{Cell viability} = \text{OD}_{\text{sample}} / \text{OD}_{\text{control}} \times 100$$

### Live and Dead Staining Analysis

Further detection of cell viability utilizing the live and dead staining kit was investigated with the fluorescent staining technique. As already described above, the same experiments were repeated until MCF-7 cancer cells were treated with various samples concentration (10 µl of 120 µg/ml) and subsequently incubated. After incubation, staining solution at a 4 µg/ml concentration was added to each well and then incubated for 20 min at 37°C. Dead and live MCF-7 cells were analyzed with CLSM using an excitation wavelength of 493 nm and 350 for PI and Hoechst 33342 and an emission wavelength of 636 nm and 461 nm for PI and Hoechst 33342, respectively.

### Antioxidant Activity in Terms of Linoleic Acid (%) Inhibition

The antioxidant activity of the green synthesized VBLE-MnO<sub>2</sub> NPs was evaluated according to the linoleic acid (%) inhibition method reported by Iqbal et al. (2005). For this purpose, 100 µg/ml concentration of each sample (green synthesized VBLE-MnO<sub>2</sub> NPs, plant extracts, and chemically synthesized VBLE-MnO<sub>2</sub> NPs) was added to the solution mixture of 99.99% ethanol (10 ml), 0.2 M sodium phosphate buffer (pH 7.0, 10 ml), and linoleic acid (0.13 ml). With DI, the total amount of the resultant mixture was increased to 25 ml and then incubated for 360 h at 40°C. The thiocyanate technique was used to assess the extent of oxidation. Each sample solution was diluted by adding 0.2 ml of each sample solution in 10 ml of ethanol (75%). Then, 0.2 ml FeCl<sub>2</sub> (20 mm in 3.5% HCl) and 0.2 ml of aqueous ammonium thiocyanate solution (30%) were added, and then, the mixture was mixed for 3 min. Measurements of the absorption maxima were made at 500 nm wavelength. The percentage inhibition (% Inhibition) of linoleic acid was determined using the formula as:

$$\% \text{Inhibition} = 100 - \left[ \frac{(\text{Absorbance of sample})}{(\text{absorbance of control})} \times 100 \right]$$

Ascorbic acid was used as an external standard, and linoleic acid was used as a control without any treatment.

### Cytobiocompatibility Analysis

The cytobiocompatibility of the green synthesized VBLE-MnO<sub>2</sub> NPs against the hMSC cell line in comparison with the CH-MnO<sub>2</sub> NPs and plant extract was evaluated *via* the MTT protocol as reported by Emam et al. (2017). The hMSC cells were kept in Dulbecco's Modified Eagle's Medium (DMEM) in an incubator which was set at 5% CO<sub>2</sub>, 95% air, and 37°C. To obtain cell confluency up to 5 × 10<sup>8</sup> cells/well, the hMSC cells were grown for 24 h at 37°C in 100 µl of DMEM in a 96-well plate. After 50 µl of green synthesized VBLE-MnO<sub>2</sub> NPs, plant extract and CH-MnO<sub>2</sub> NPs at a concentration of 120 µg/ml were added in each well separately containing cultured hMSC cells, and the plate was further incubated for 24 h at 37°C. The plate was then centrifuged to remove the supernatant and rinsed with PBS solution. A total of 15 µl of MTT labeling agent (0.5 mg/ml) was then poured into each well; the plate was then put in an incubator for 4 h at 37°C. A total of 150 µl of DMSO was added to each well to solubilize the undissolved crystals of formazan. The optical density (OD) of formazan product in each well was measured at 570 nm using a Varian Eclipse spectrophotometer. The percentage of cell viability was calculated using the following formula:

$$\% \text{Cell viability} = \text{OD}_{\text{sample}} / \text{OD}_{\text{control}} \times 100$$

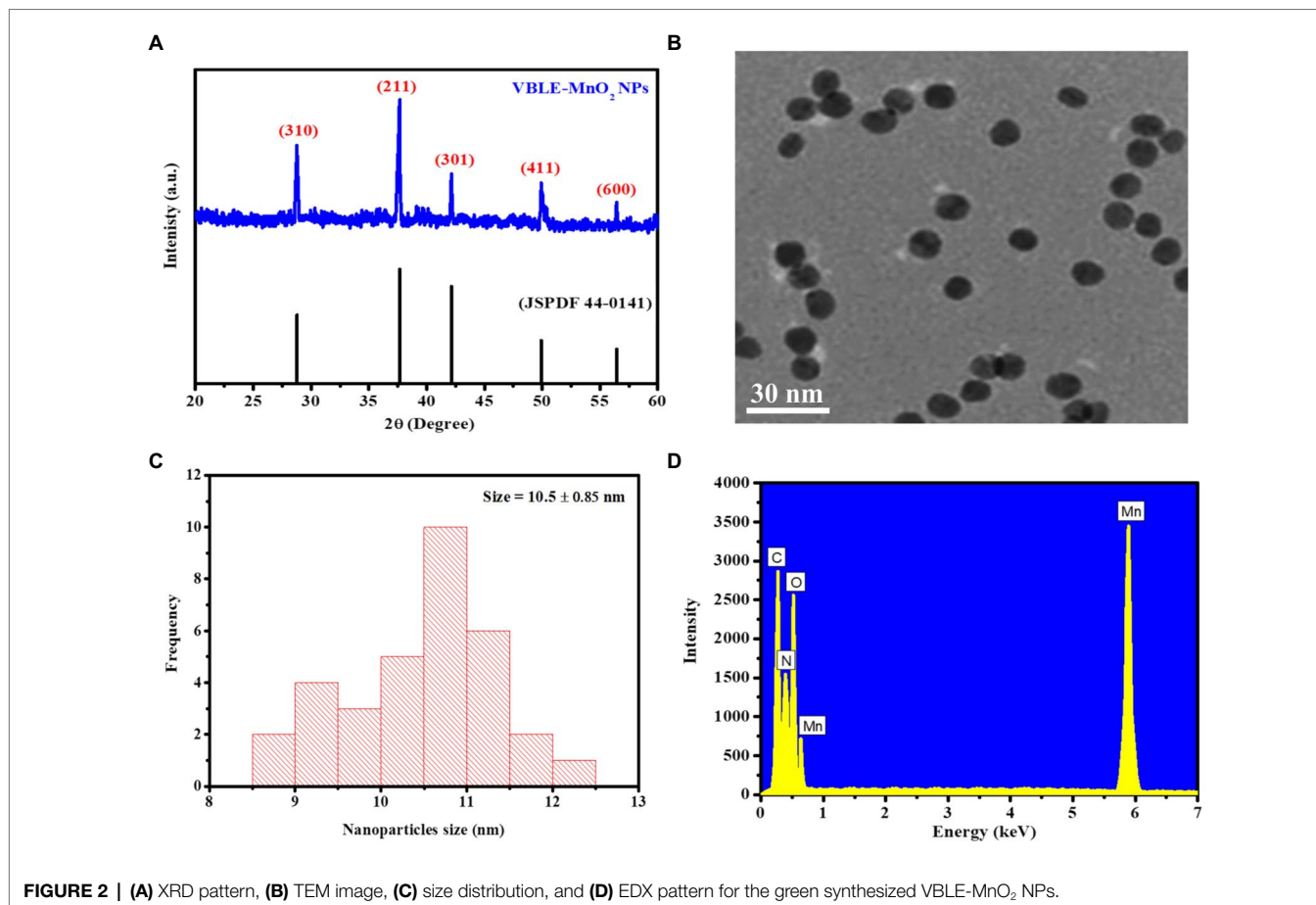
### Statistical Analysis

All trials were conducted in triplicate, and the findings are given as mean ± standard deviation. To ascertain the statistical significance, we used ANOVA with a predetermined significance level (0.05).

## RESULTS AND DISCUSSION

### Synthesis Mechanism

For the fabrication of VBLE-MnO<sub>2</sub> NPs, the leaf extract of *V. betonicifolia* was utilized as a reducing and capping agent. The formation of VBLE-MnO<sub>2</sub> NPs was visually tracked by observing the color change caused by the addition of a precursor to leaf extract. The reaction mixture's color shift from yellowish green to brownish indicated the formation of the required manganese dioxide NPs. This color shift occurred as a consequence of the nanoparticle's surface plasmon resonance action. Several reports demonstrate that the leaves extract of *V. betonicifolia* is a rich source of several biogenic phytochemicals, including alkaloids, flavonoids, tannins, phenolic compounds, saponins, and triterpenoids [14–17]. During the biosynthesis process, these phytochemicals might be functioned as reducing the manganese ions to zero-valent species *via* reduction and oxidation reaction with the production of keto form products. Further, other secondary metabolites (surfactants, proteins, alkaloids, etc.) present in the leaf extract of the *V. betonicifolia*



simultaneously stabilized and capped the zero-valent species of Mn<sup>0</sup>. During air-drying and calcination at 200°C, zero-valent species of Mn<sup>0</sup> would be readily oxidized and converted into MnO<sub>2</sub> nanoparticles capped with phytomolecules of plant leaf extract (Figure 1). Similar green synthesis mechanism of NPs using different plant extract was also reported by Dzul-Erosa et al. (2018); Khalafi et al. (2019); Rafique et al. (2019); Ciorîță et al. (2020); Gurgur et al. (2020); López and Antuch (2020); Khan et al. (2020b).

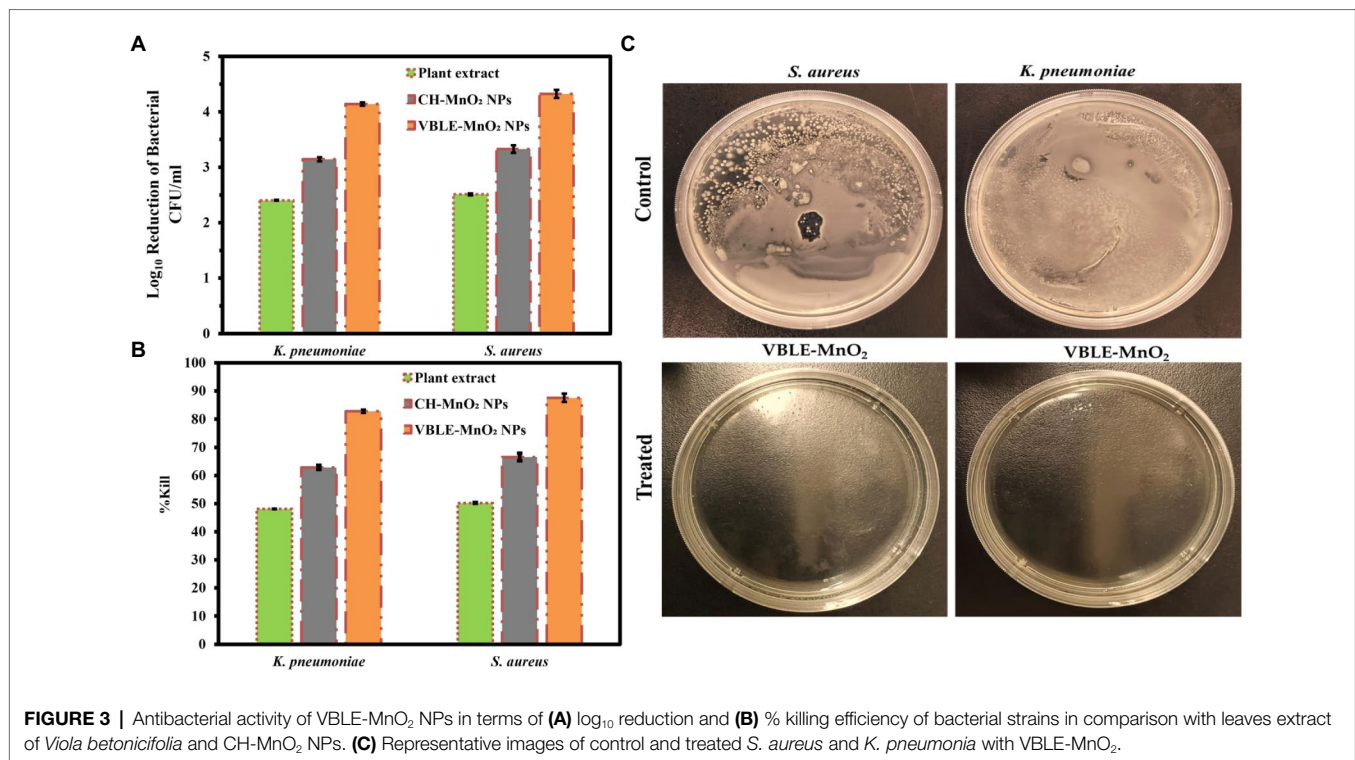
## Characterization

XRD analysis was carried out to analyze the crystallinity of the VBLE-MnO<sub>2</sub> NPs synthesized using the leaves extract of *V. betonicifolia*. Figure 2A shows an XRD pattern of the VBLE-MnO<sub>2</sub> NPs. XRD pattern demonstrates five distinguish peaks at  $2\theta = 28.78^\circ$ ,  $37.66^\circ$ ,  $42.14^\circ$ ,  $49.90^\circ$ , and  $56.44^\circ$ , indexed to (310), (211), (301), (411), and (600) crystal plane of VBLE-MnO<sub>2</sub> NPs (JSPDF 44-0141; He et al., 2018, 2019; Wan et al., 2019). Moreover, the XRD pattern indicates that the VBLE-MnO<sub>2</sub> NPs are highly crystalline, as evident from the intensity of the peaks. Figure 2B presents the TEM images of VBLE-MnO<sub>2</sub> NPs. The TEM image depicts that the synthesized VBLE-MnO<sub>2</sub> NPs are spherical with homogeneous dispersity. The particle size of the synthesized VBLE-MnO<sub>2</sub> NPs was estimated to be  $10.5 \pm 0.85$  nm using Zetasizer Dynamic Light Scattering,

as shown in Figure 2C. To determine the chemical composition of the VBLE-MnO<sub>2</sub> NPs, the EDX analysis was then conducted. Figure 2D shows the EDX pattern. EDX spectra indicate four characteristics peaks corresponding to carbon, nitrogen, oxygen, and manganese at 0.27 keV, 0.39 keV, 0.52 keV, and 5.8 keV, respectively. A small peak at 0.63 keV attribute to Mn is also evident in EDX spectra (Panahi-Kalamuei et al., 2016; Srither et al., 2016; Ogunyemi et al., 2019). The EDX peaks (C and N) might be attributed to the adsorption of secondary metabolites from *V. betonicifolia* leaves extract on the surface of VBLE-MnO<sub>2</sub> NPs (Ciorîță et al., 2020). Thus, these characterization findings confirmed the effective synthesis of VBLE-MnO<sub>2</sub> NPs using a leaf extract of *V. betonicifolia*.

## Antibacterial Activity

Antibacterial activity of VBLE-MnO<sub>2</sub> NPs was determined in terms of log<sub>10</sub> reduction and % killing efficiency of bacterial strains compared to leaves extract of *V. betonicifolia* and CH-MnO<sub>2</sub> NPs. The results are presented in Figures 3A–C. The outcomes have been shown that the synthesized VBLE-MnO<sub>2</sub> NPs displayed  $4.14 \pm 0.03$  and  $4.65 \pm 0.07$  log<sub>10</sub> reductions in CFU of *K. pneumoniae* and *S. aureus*, respectively, with more than 80% killing efficiency. On the other hand, CH-MnO<sub>2</sub> NPs demonstrated the least antibacterial activity (log<sub>10</sub> reductions  $3.14 \pm 0.04$  and



3.33 ± 0.08 against *K. pneumoniae* and *S. aureus*, respectively) than VBLE-MnO<sub>2</sub> NPs, as shown in **Figures 3A,B**. It is worth noting that the leaves extract of *V. betonicifolia* has shown significant antibacterial behavior (log<sub>10</sub> reductions >2.35) and more than 45 percent killing performance against all bacteriological species tested. This indicates that the leaves extract of *V. betonicifolia* possesses pharmacologically important phytochemicals capable of killing bacterial strains effectively (Feyzabadi et al., 2017; Rizwan et al., 2019). Additionally, we conducted an ANOVA test on the antibacterial findings, which showed a significant difference of  $p < 0.005$ .

### LIVE and DEAD Staining Assay

LIVE and DEAD staining assay was used to evaluate the interaction of synthesized VBLE-MnO<sub>2</sub> NPs with cells and subsequent cell death upon labeling with Hoechst 33342 and PI. The permeability of the bacterial membrane to these dyes is dependent on the cellular membrane's potential, which allows for the differentiation of alive and dead cells. Hoechst 33342 is a membrane-permeant dye can stain both alive and dead cells by interlacing DNA, while PI is a membrane-impermeant dye that permeates only through dead cells' perforated membranes and can stain only dead cells (Arakha et al., 2015; Ramalingam et al., 2016). As illustrated in **Figures 4A,C**, the untreated *K. pneumoniae* and *S. aureus*, stained only with Hoechst 33342, suggesting that they were intact and alive. At the same time, VBLE-MnO<sub>2</sub> NPs treated cells fluoresced red (**Figures 4B,D**). This revealed that VBLE-MnO<sub>2</sub> NPs triggering cell death had an effect on the integrity and permeability of the cell membrane.

### Reactive Oxygen Species Generation in Bacteria Treated With VBLE-MnO<sub>2</sub>

Oxidative stress caused by intracellular ROS production has been shown to destroy microbial strains (Kim et al., 2007). Metal nanoparticles (NPs) interact with bacteria to produce ROS, which can lead to oxidative stress inside the cell and the destruction of organelles and biomolecules. **Figure 5** depicts the results of the CellROX<sup>®</sup>Green test, which was used to assess oxidative stresses in microbial cells following treatment with VBLE-MnO<sub>2</sub> NPs. No intracellular ROS species were produced in either bacterial cell under control. Both bacteria treated with VBLE-MnO<sub>2</sub> produced ROS comparable to that produced by H<sub>2</sub>O<sub>2</sub>. These findings suggest that one explanation for the outstanding antibacterial activity of the VBLE-MnO<sub>2</sub> produced is the production of ROS, which causes bacterial cells to die. Graphical presentation of ROS production mechanism in bacterial cells due to VBLE-MnO<sub>2</sub> NPs is shown in **Figure 5**.

### Antibacterial Mechanism

Additionally, the superior antibacterial action of VBLE-MnO<sub>2</sub> NPs can be due to the synergy influence of the nanoparticle's physical characteristics and the adsorption of biologically active phytochemicals from the leaves extract of *V. betonicifolia* on their surface (Huang et al., 2011; Khan et al., 2018, 2020a,b, 2021a,b). The results were further demonstrated that the synthesized VBLE-MnO<sub>2</sub> NPs appeared more active toward the Gram-positive in contrast to that of Gram-negative bacteriological species. This may be due to structural and compositional variations between Gram-negative and

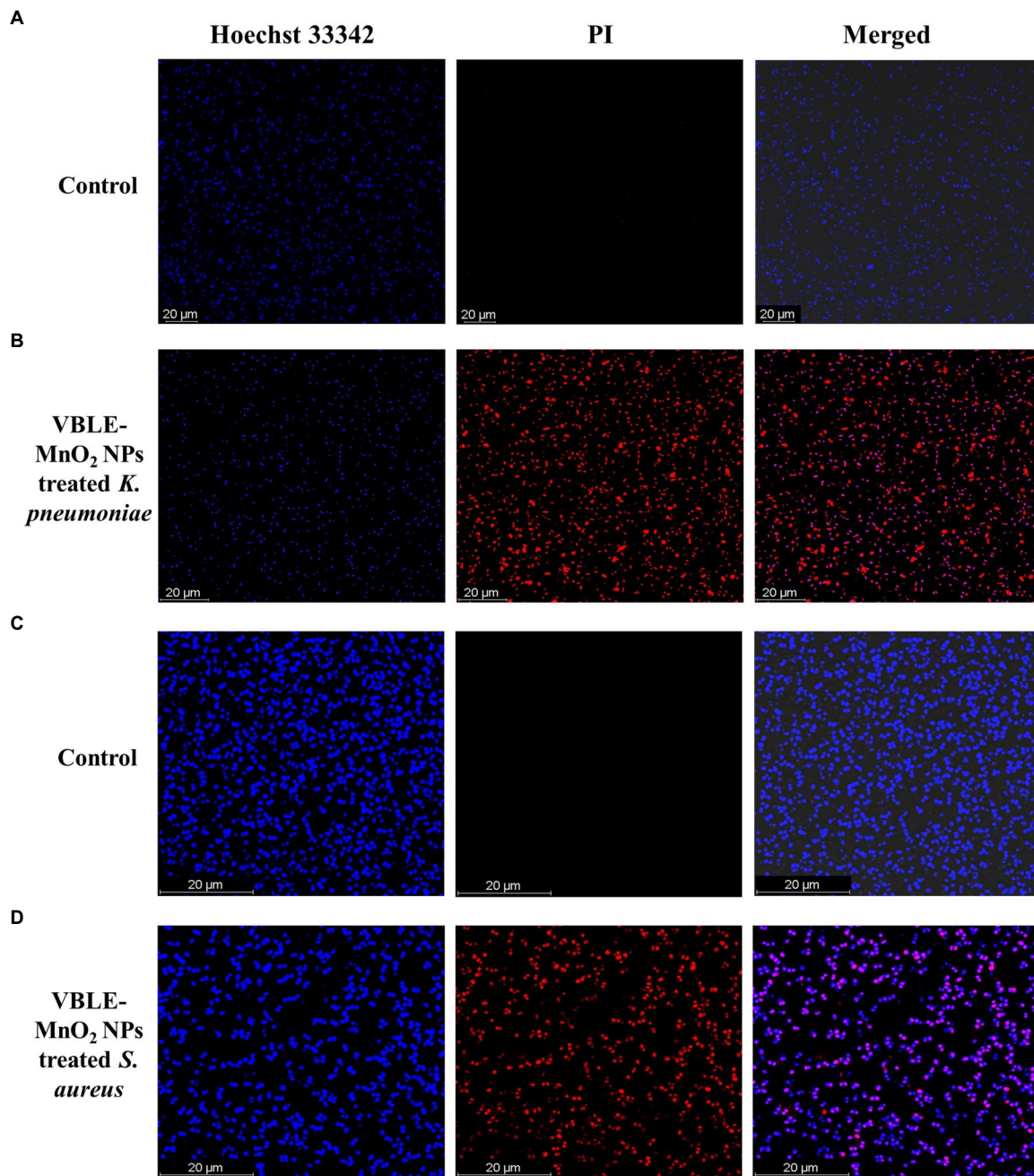


**FIGURE 4** | CLSM images of untreated [control (A,C)] and treated (B,D) bacteria with synthesized VBLE-MnO<sub>2</sub> NPs. Red represents dead bacterial cells.

Gram-positive bacterial strains' cell walls (Figures 6A,B; Bindhu and Umadevi, 2014; Muthukumar et al., 2016; Boomi et al., 2019). Manjula et al. and Kunkalekar et al. were also reported the same more inhibitory effect of MnO<sub>2</sub> NPs toward Gram-positive than Gram-negative bacteria (Kunkalekar et al., 2013; Manjula et al., 2019).

Numerous reports have shown that the antibacterial effect of nanomaterials is mostly due to physical (e.g., lipid molecule disintegration) and chemical (e.g., oxidative stress) deterioration (Du et al., 2020). The synergy of antibacterial activity was

defined in this study using a two-step approach: (1) generation of reactive oxygen species (Figures 5, 6C) and (1) membrane damage, leakage of electrolytes and intracellular contents, and decrease in ATPase activity, all of which contribute to bacterial death (Figures 4, 6C).

### Antifungal Activity

In contrast to leaves extract of *V. betonicifolia* and CH-MnO<sub>2</sub> NPs, the antifungal activity of synthesized VBLE-MnO<sub>2</sub> NPs

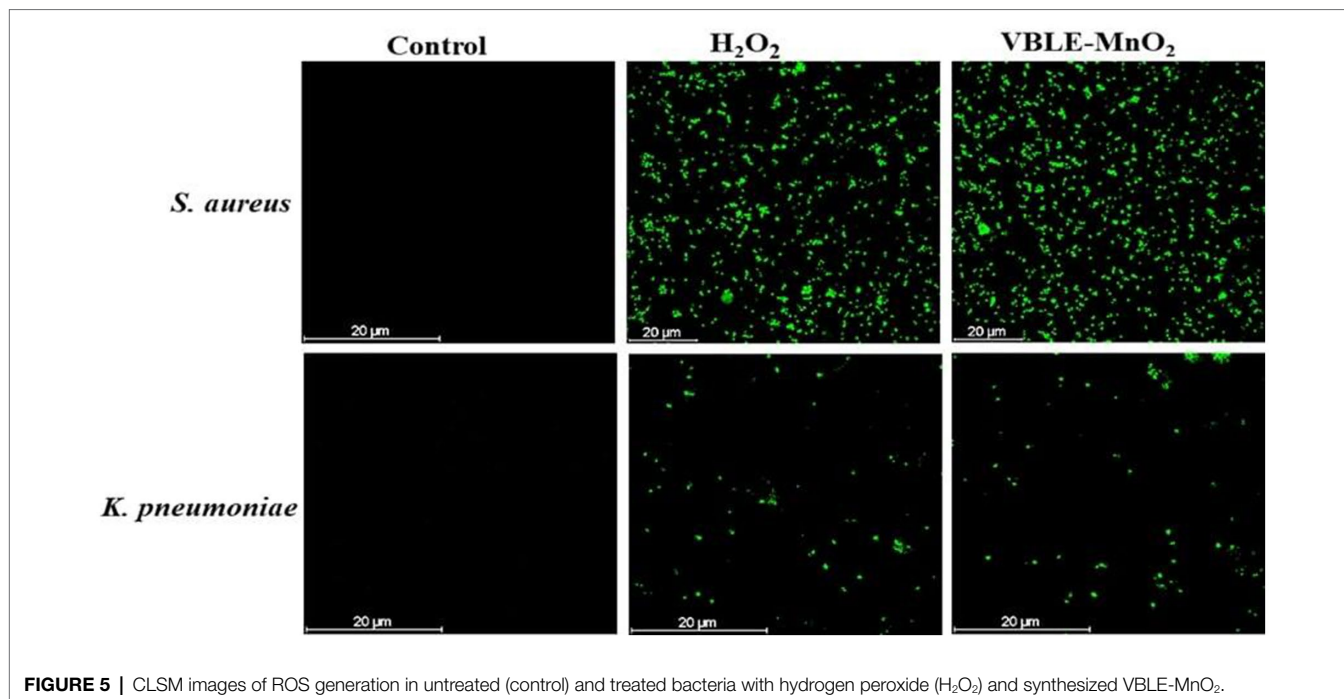


**FIGURE 5** | CLSM images of ROS generation in untreated (control) and treated bacteria with hydrogen peroxide (H<sub>2</sub>O<sub>2</sub>) and synthesized VBLE-MnO<sub>2</sub>.

was determined in terms of log<sub>10</sub> reduction and % killing efficiency of mycological strains. **Figures 7A,B** illustrate the findings. The results indicated that the synthesized VBLE-MnO<sub>2</sub> NPs significantly reduced the CFU of *A. flavus*, *T. harzianum*, and *A. fumigatus* by  $4.05 \pm 0.06$ ,  $4.32 \pm 0.07$ , and  $4.63 \pm 0.05$  log<sub>10</sub> reductions, respectively, with a killing efficiency of more than 82 percent. CH-MnO<sub>2</sub> NPs, on the other hand, demonstrated significantly lower antifungal activity than VBLE-MnO<sub>2</sub> NPs, as shown in **Figures 7A,B**. Furthermore, we conducted an ANOVA test on the antifungal activity results, which exhibited a significant difference of  $p < 0.002$ . It is worth noting that the leaves extract of *V. betonicifolia* also demonstrated substantial antifungal activity and percent killing efficiency against all tested mycological strains. This indicates that the *V. betonicifolia* leaf extract contains biologically active phytochemicals that are particularly effective at destroying fungal strains (Katoch et al., 2017). Additionally, the superior antifungal activity of VBLE-MnO<sub>2</sub> NPs can be due to the synergistic impact of the nanoparticle's physical properties and the adsorbed biologically active phytochemicals from the leaves extract of *V. betonicifolia* on their surface. The similar antifungal results were also reported with the green synthesized MnO NPs using leaf extract of *Abutilon indicum* by Khan et al. (2020b).

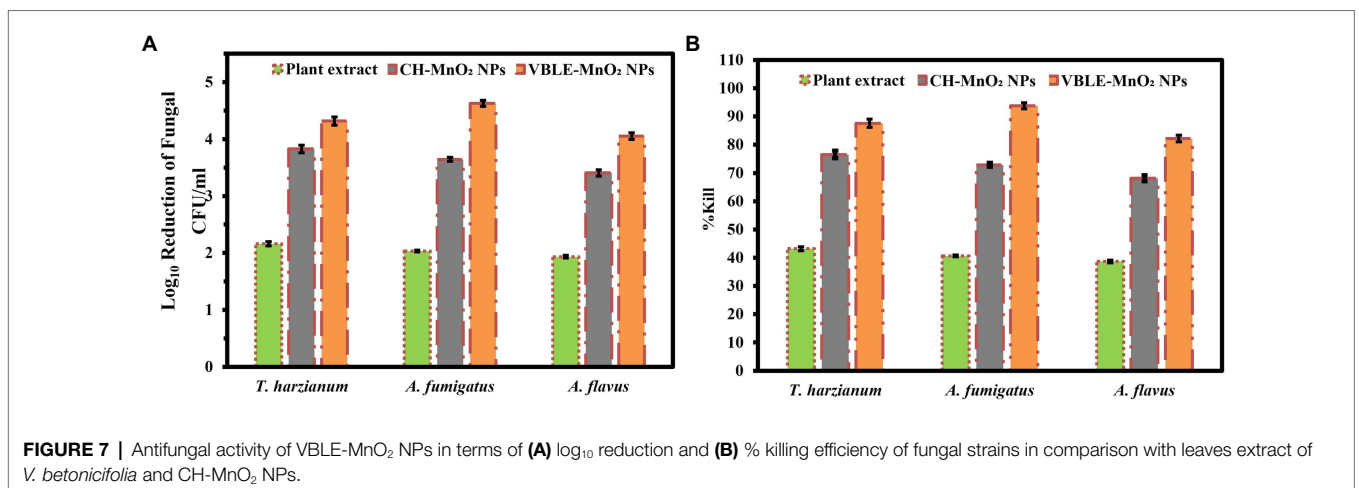
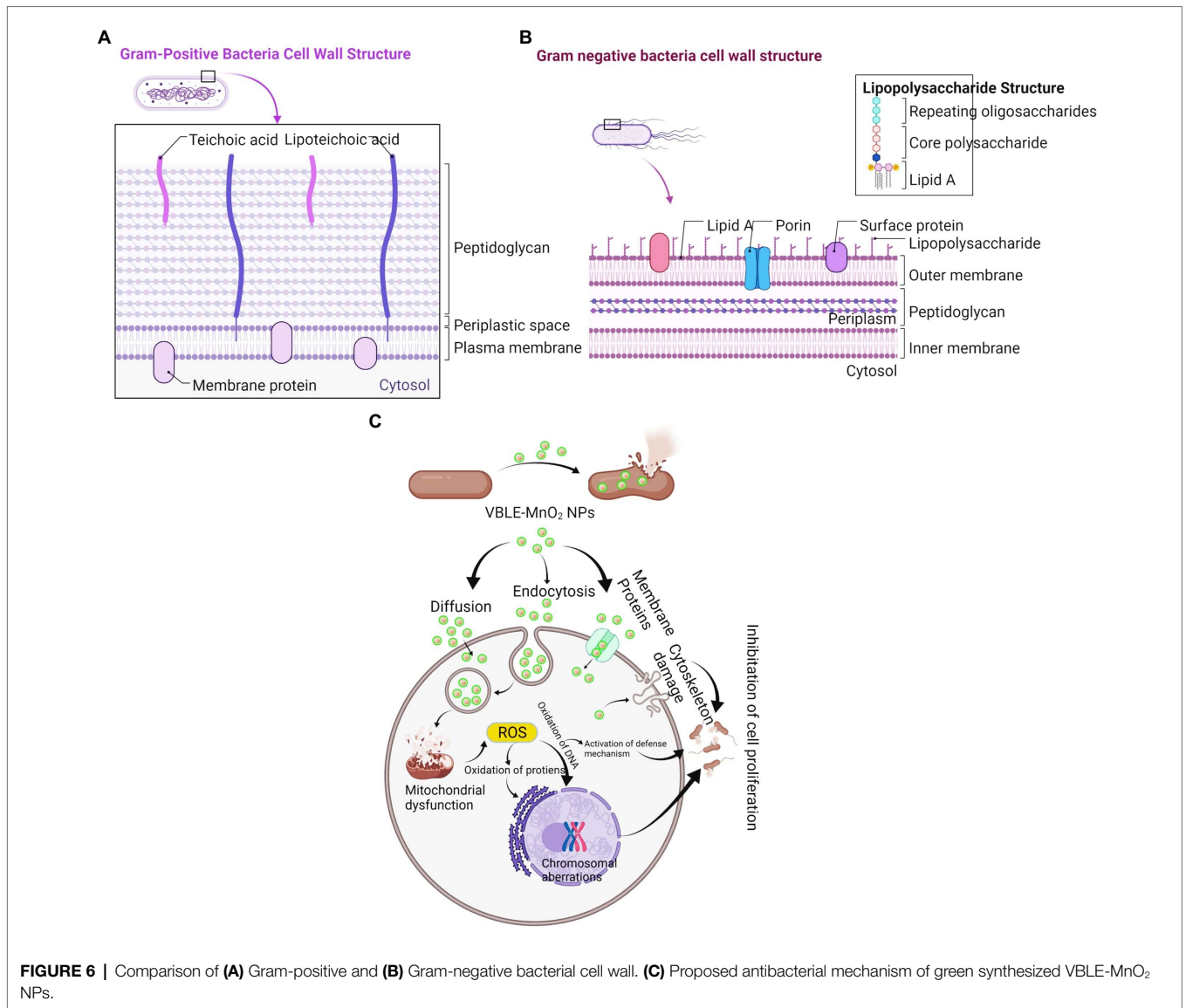
### Biofilm Inhibition Investigations

The biofilm inhibition activity of VBLE-MnO<sub>2</sub> NPs was evaluated against infectious bacterial and mycological species in contrast to *V. betonicifolia* leaves extract and CH-MnO<sub>2</sub> NPs. **Figures 8A,B** illustrate the findings. The findings indicate that the VBLE-MnO<sub>2</sub> NPs exhibited substantial biofilm inhibitory activity, inhibiting the production of biofilms of both bacterial and mycological strains. Although CH-MnO<sub>2</sub> NPs inhibited the

production of biofilms in both microbial species but were less than VBLE-MnO<sub>2</sub> NPs synthesized with *V. betonicifolia* leaves extract. Moreover, the *V. betonicifolia* leaves extract also demonstrated good biofilm inhibition performance, as evident from **Figures 8A,B**. In addition, we performed an ANOVA test on the biofilm inhibition activity data against both of fungal and bacterial strains, which revealed a significant difference of  $p < 0.002$  and  $p < 0.001$ , respectively. The remarkable biofilm inhibition efficiency of the synthesized VBLE-MnO<sub>2</sub> NPs may be a result of the synergy between their physical properties and the incorporation of phytochemicals from *V. betonicifolia* leaves extract on the nanoparticle's surface.

### Cytotoxic Potential Against MCF-7 Carcinoma Cells

The cytotoxic potential of VBLE-MnO<sub>2</sub> NPs was determined by comparing them to *V. betonicifolia* leaves extract and CH-MnO<sub>2</sub> NPs. The findings indicated that all samples exhibited dose-dependent therapeutic effectiveness (**Figure 9A**). The maximum inhibitory effects on MCF-7 melanoma cells were observed when all samples were concentrated to 120 μg/ml. The VBLE-MnO<sub>2</sub> NPs displayed excellent cytotoxic activity in comparison with *V. betonicifolia* leaves extract and CH-MnO<sub>2</sub> NPs at all dose levels. The extraordinary cytotoxic activity of the produced VBLE-MnO<sub>2</sub> NPs might be attributed by a synergy between their physical characteristics and the inclusion of phytochemicals from *V. betonicifolia* leaves extract on the NP's surface. It is worth mentioning that the leaves extract of *V. betonicifolia* also exhibited effective cytotoxic activity against MCF-7 carcinoma cells. This shows that the leaves extract of *V. betonicifolia* contains phytochemicals of pharmacological



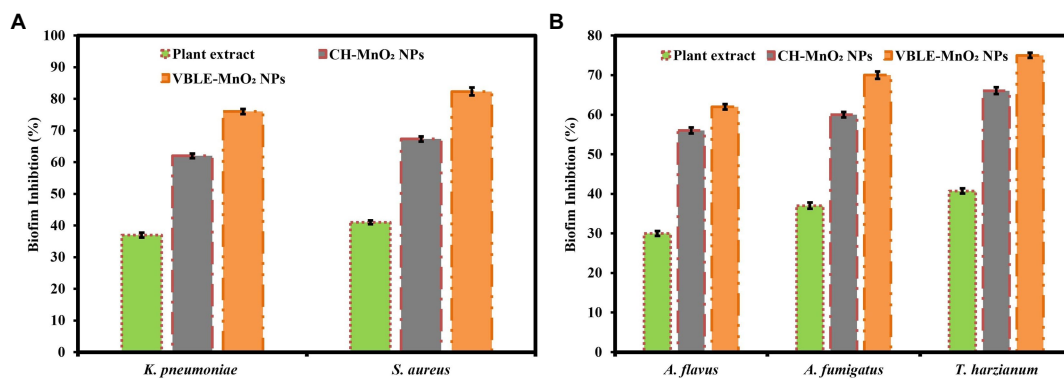


**FIGURE 8 |** Biofilm inhibition performance of the synthesized VBLE-MnO<sub>2</sub> NPs against the (A) bacterial and (B) fungal strains in comparison with *V. betonicifolia* leaves extract and CH-MnO<sub>2</sub> NPs.

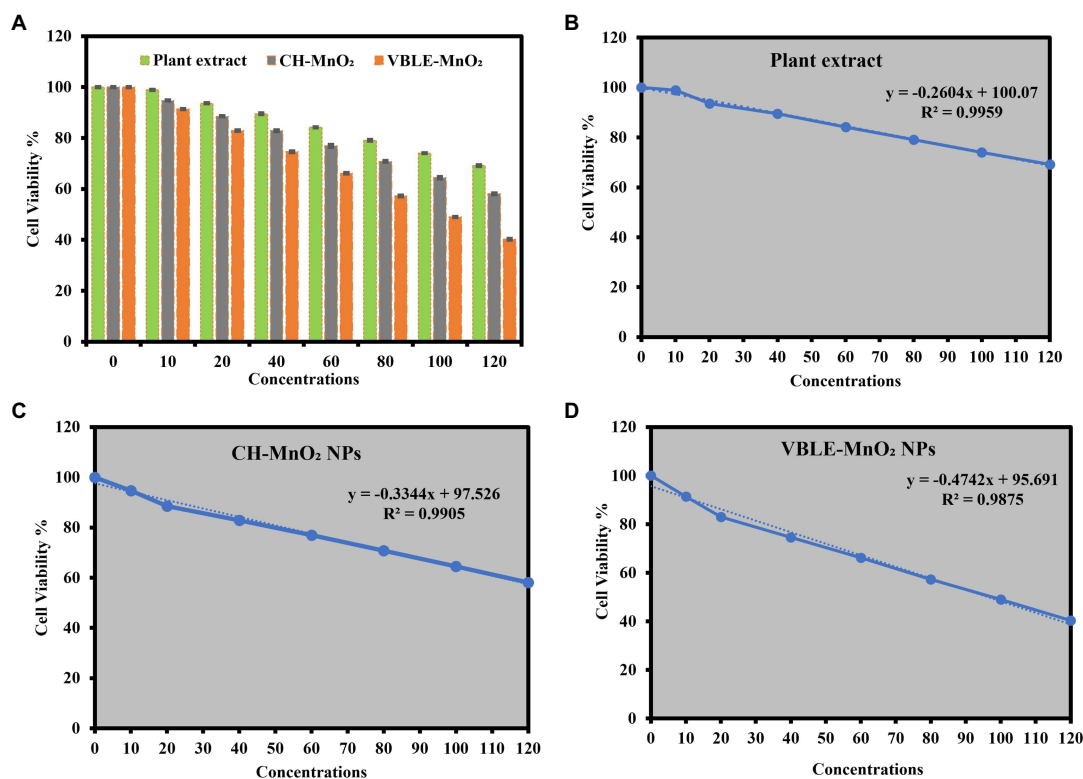


**FIGURE 9 |** (A) Cytotoxic potential in terms of cell viability percentage against MCF-7 carcinoma cells treated with *V. betonicifolia* leaves extract, CH-MnO<sub>2</sub> NPs, and VBLE-MnO<sub>2</sub> NPs. Linear plot and regression coefficient between the cell viability % of the MCF-7 carcinoma cells with different concentrations of (B) *V. betonicifolia* leaves extract, (C) CH-MnO<sub>2</sub> NPs, and (D) VBLE-MnO<sub>2</sub> NPs.

significance capable of efficiently killing cancerous cells. Moreover, linearity has been observed between the cell viability % of the MCF-7 carcinoma cells with different concentrations of *V. betonicifolia* leaves extract, CH-MnO<sub>2</sub> NPs, and VBLE-MnO<sub>2</sub> NPs as shown in **Figures 9B–D**, respectively. We further performed ANOVA test on cytotoxic results of three groups against different concentrations of 0, 10, 20, 40, 60, 80, 100, and 120 µg/ml and the results

revealed the statistical difference by  $p > 0.05$ ,  $p < 0.001$ ,  $p < 0.003$ ,  $p < 0.004$ ,  $p < 0.008$ ,  $p < 0.001$ ,  $p < 0.005$ , and  $p < 0.006$ , respectively. Our synthesized VBLE-MnO<sub>2</sub> NPs appeared more active toward killing the carcinoma cells as compared to green synthesized Ag-MnO<sub>2</sub> NPs previously reported by Ciorîță et al. (2020) but comparable to the NPs reported by Khan et al. (2020b). The similar dose-dependent cytotoxic activity was also reported by Khan et al. (2020b).

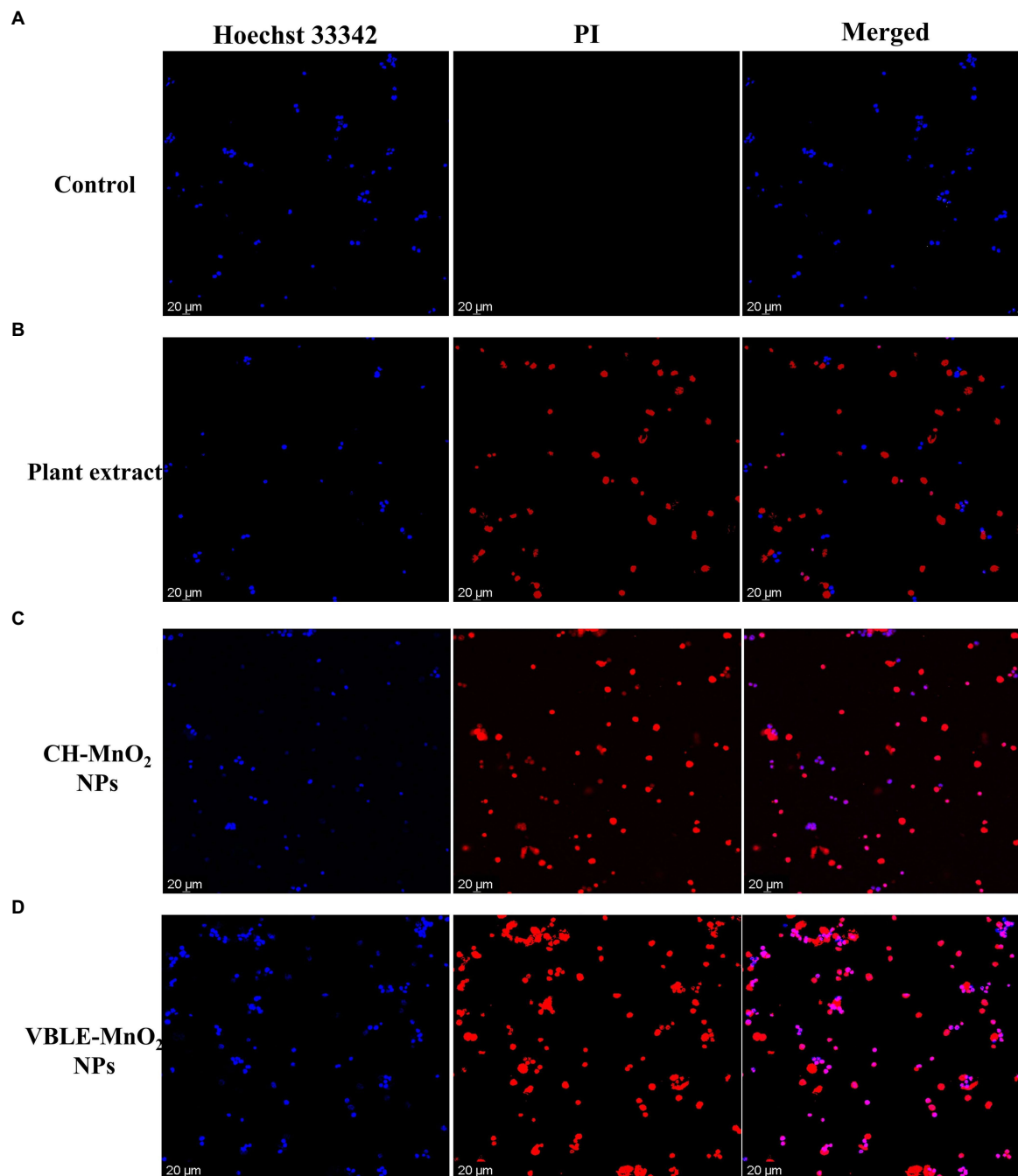
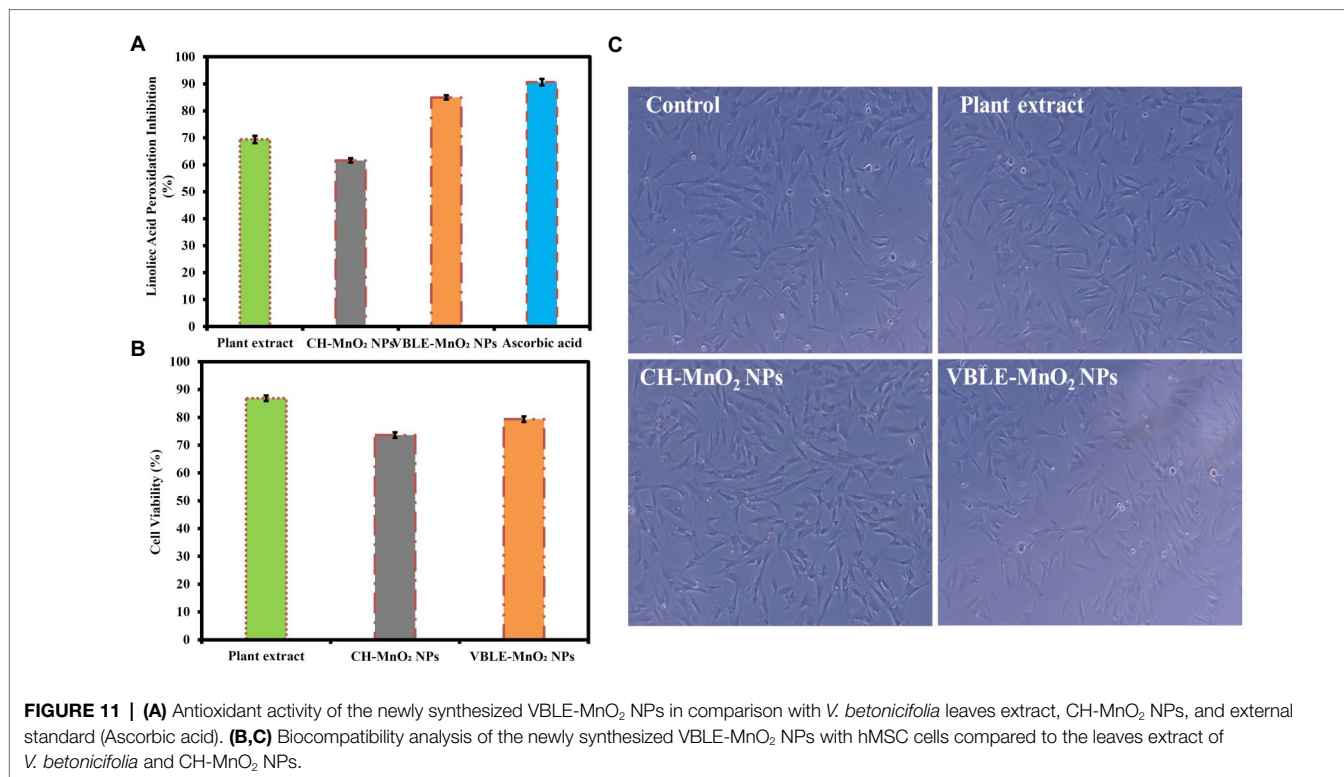


**FIGURE 10 |** CLSM images of the live and dead MCF-7 cancer cells stained with Hoechst 33342 and PI dye before **(A)** control and after treatment with **(B)** plant extract, **(C)** CH-MnO<sub>2</sub> NPs, and **(D)** VBLE-MnO<sub>2</sub> NPs.

### Live and Dead Staining

CLSM was further used to confirm the cytotoxicity against MCF-7 cancerous cells utilizing the live and dead fluorescence staining experiment. **Figures 10A–D** exhibit living, and deceased MCF-7 cancerous cells dyed with Hoechst 33342 and PI dye, respectively. Hoechst 33342 is a membrane-permeant dye can stain both alive and dead cells by interlacing

DNA, while PI is a membrane-impermeant dye that permeates only through dead cells' perforated membranes and can stain only dead cells. The findings showed that VBLE-MnO<sub>2</sub> NPs had the greatest cytotoxic impact on MCF-7 carcinoma cells, killing almost of malignant cells, while CH-MnO<sub>2</sub> NPs had a moderate toxic impact on MCF-7 cancer cells. It is worth noting that leaf extract was similarly hazardous



to MCF-7 cancer cells, suggesting that *V. betonicifolia* leaves extract contains pharmacologically active phytochemicals. These findings are compatible with the findings of MTT analyses.

## Antioxidant Activity

Antioxidant activity of the newly synthesized VBLE-MnO<sub>2</sub> NPs was investigated in comparison with the leaves extract of *V. betonicifolia*, CH-MnO<sub>2</sub> NPs, and external standard (ascorbic acid). **Figure 11A** illustrates the findings. The anti-linoleic acid peroxidation activity of newly synthesized VBLE-MnO<sub>2</sub> NPs was superior ( $84.94 \pm 0.77\%$ ) to that of *V. betonicifolia* leaves extract and CH-MnO<sub>2</sub> NPs, although a little less than that of ascorbic acid ( $90.57 \pm 1.21\%$ ). On the other hand, CH-MnO<sub>2</sub> NPs exhibited the lowest antioxidant function, exhibiting the lowest percentage of anti-linoleic acid peroxidation ( $61.61 \pm 0.79\%$ ). Additionally, the leaves extract of *V. betonicifolia* demonstrated superior antioxidant function by inhibiting linoleic acid peroxidation ( $69.37 \pm 1.37\%$ ) as compared to CH-MnO<sub>2</sub> NPs. These findings suggested that *V. betonicifolia* leaves extract contains a high concentration of natural antioxidants (Muhammad et al., 2013b; Rizwan et al., 2019). Furthermore, the inclusion of phytochemicals from *V. betonicifolia* leaves extract on the nanoparticle's surface could be responsible for the VBLE-MnO<sub>2</sub> NPs' superior antioxidant activity. We performed an ANOVA test on the antioxidant findings and determined that they were statistically significant at  $p < 0.004$ . The similar enhanced antioxidant activity of the green synthesized NPs was also reported by Khan et al. (2020a); Shahid et al. (2021).

## Biocompatibility Evaluation

The biocompatibility of VBLE-MnO<sub>2</sub> NPs was assessed with the hMSC cells *in vitro* compared to the *V. betonicifolia* leaves extract and CH-MnO<sub>2</sub> NPs. The results are expressed as a percentage of cell viability, as shown in **Figure 11B**. The findings indicated that CH-MnO<sub>2</sub> NPs had the lowest cell viability percentage ( $73.54 \pm 0.82\%$ ). On the other side, newly synthesized VBLE-MnO<sub>2</sub> NPs demonstrated a cell viability percentage ( $79.33 \pm 0.75\%$ ) with hMSC cells. Additionally, it is noteworthy to mention that the extract of *V. betonicifolia* leaves contains biocompatible secondary metabolites that demonstrated excellent biocompatibility (cell viability percentage  $86.84 \pm 0.85\%$ ) with hMSC cells. It has been reported that different solvent extracts of *V. betonicifolia* are safe to use and have no toxic effects (Muhammad et al., 2012, 2013c; Rizwan et al., 2019). We used an ANOVA test to determine the statistical significance of the biocompatibility findings and discovered a  $p < 0.007$  significance level.

We next examined the morphological changes in hMSC cells treated with VBLE-MnO<sub>2</sub> NPs, plant extract, and CH-MnO<sub>2</sub> NPs at a 120 µg/ml concentration using an inverted microscope. The inverted micrograph of hMSC cells is shown in **Figure 11C**. The photographs demonstrate that following treatment with plant extract and VBLE-MnO<sub>2</sub> NPs, the morphology of hMSC cells remained comparable to that of the control (untreated cells). On the other hand, CH-MnO<sub>2</sub> NPs caused toxicity in hMSC cells, reducing their volume and cytoplasm, and altering their shape. The viability of cells and the inverted microscopy findings were found to be consistent. As a result, it can be inferred that phytochemicals contained in the leaves extract

of *V. betonicifolia* may be responsible for the VBLE-MnO<sub>2</sub> NPs' enhanced cytobiocompatibility. The similar enhanced biocompatibility of the green synthesized NPs with various normal cell lines was also reported by Ciorîță et al. (2020) and Khan et al. (2020a,b, 2021b).

## CONCLUSION

The manganese dioxide NPs (VBLE-MnO<sub>2</sub> NPs) were synthesized using the leaves extract of *V. betonicifolia* very first time, in which the plant's secondary metabolites function as both reducing and capping agents. The synthesized VBLE-MnO<sub>2</sub> NPs were successfully characterized with different spectroscopic techniques. The synthesized VBLE-MnO<sub>2</sub> NPs were investigated for different biological activities (antioxidant, cytotoxicity, antibacterial, antifungal, and biofilm inhibition). The results were demonstrated that the synthesized VBLE-MnO<sub>2</sub> NPs presented excellent antibacterial, antifungal, and biofilm inhibition performance against all the tested microbial species compared to plant leaves extract and commercially purchased chemically synthesized manganese dioxide NPs (CH-MnO<sub>2</sub> NPs). Moreover, they also exhibited significant antioxidant potential, which was comparable to the external standard; however, it was higher than plant leaves extract and CH-MnO<sub>2</sub> NPs. The synthesized CH-MnO<sub>2</sub> NPs displayed good cytobiocompatibility with hMSC cells compared to CH-MnO<sub>2</sub> NPs. The enhanced antioxidant, cytobiocompatibility, antibacterial, antifungal, biofilm inhibition, and cytotoxic efficacy of VBLE-MnO<sub>2</sub> NPs as compared to CH-MnO<sub>2</sub> NPs might be attributed to the synergistic effect of the nanoparticle's physical properties and the adsorbed biologically active phytomolecules from the leaves extract of *V. betonicifolia* on their surface. Thus, our work offers a unique environmentally sustainable technique for the manufacture of nanomaterials bestowed with enhanced and/or additional therapeutic properties obtained from their herbal sources. Furthermore, more study should be conducted to determine the efficacy and dose response biocompatibility of VBLE-MnO<sub>2</sub> NPs in therapeutic interventions. The VBLE-MnO<sub>2</sub> NPs

synthesized in this research could be utilized to provide antibacterial coatings for medical devices, such as catheters, tubing, sensors, and bandages, thereby lowering the incidence of pathogenic bacteriological and mycological infections induced by biomaterials and medical implants.

## DATA AVAILABILITY STATEMENT

The raw data supporting the conclusions of this article will be made available by the authors, without undue reservation.

## AUTHOR CONTRIBUTIONS

HL and XZ: conceptualization, methodology, software, validation, formal analysis, and investigation. SK, WL, and LW: resources, data curation, writing—original draft preparation, writing—review and editing, visualization, supervision, and project administration. WL and LW: funding acquisition. All authors have read and agreed to the published version of the manuscript.

## FUNDING

This research was funded by the National Natural Science Foundation of China (81600900) and the Science Foundation of Stomatological Hospital, Southern Medical University (PY2019013), and the Postdoctoral sustentation fund of Shunde district, Foshan city.

## ACKNOWLEDGMENTS

We would like to thank the National Natural Science Foundation of China (81600900) and the Science Foundation of Stomatological Hospital, Southern Medical University (PY2019013), and the Postdoctoral sustentation fund of Shunde district, Foshan city.

## REFERENCES

- Abbasi, B. A., Iqbal, J., Mahmood, T., Ahmad, R., Kanwal, S., and Afridi, S. (2019a). Plant-mediated synthesis of nickel oxide nanoparticles (NiO) via geranium wallichianum: characterization and different biological applications. *Mater. Res. Express* 6:0850a7. doi: 10.1088/2053-1591/ab23e1
- Abbasi, B. A., Iqbal, J., Mahmood, T., Qyyum, A., and Kanwal, S. (2019b). Biofabrication of iron oxide nanoparticles by leaf extract of *Rhamnus virgata*: characterization and evaluation of cytotoxic, antimicrobial and antioxidant potentials. *Appl. Organomet. Chem.* 33:e4947. doi: 10.1002/aoc.4947
- Al-Radadi, N. S. (2019). Green synthesis of platinum nanoparticles using Saudi's dates extract and their usage on the cancer cell treatment. *Arab. J. Chem.* 12, 330–349. doi: 10.1016/j.arabjc.2018.05.008
- Arakha, M., Saleem, M., Mallick, B. C., and Jha, S. (2015). The effects of interfacial potential on antimicrobial propensity of ZnO nanoparticle. *Sci. Rep.* 5:9578. doi: 10.1038/srep09578
- Bindhu, M. R., and Umadevi, M. (2014). Antibacterial activities of green synthesized gold nanoparticles. *Mater. Lett.* 120, 122–125. doi: 10.1016/j.matlet.2014.01.108
- Boomi, P., Ganesan, R. M., Poorani, G., Gurumallesh Prabu, H., Ravikumar, S., and Jeyakanthan, J. (2019). Biological synergy of greener gold nanoparticles by using *Coleus aromaticus* leaf extract. *Mater. Sci. Eng. C* 99, 202–210. doi: 10.1016/j.msec.2019.01.105
- Chandran, S. P., Chaudhary, M., Pasricha, R., Ahmad, A., and Sastry, M. (2006). Synthesis of gold nanotriangles and silver nanoparticles using *Aloe vera* plant extract. *Biotechnol. Prog.* 22, 577–583. doi: 10.1021/bp0501423
- Choi, K.-H. H., Nam, K. C., Lee, S.-Y. Y., Cho, G., Jung, J.-S. S., Kim, H.-J. J., et al. (2017). Antioxidant potential and antibacterial efficiency of Caffeic acid-functionalized ZnO nanoparticles. *Nano* 7:148. doi: 10.3390/nano7060148
- Ciorîță, A., Suciuc, M., Macavei, S., Kacso, I., Lung, I., Soran, M. L., et al. (2020). Green synthesis of Ag-MnO<sub>2</sub> nanoparticles using *chelidonium majus* and *vinca minor* extracts and their *in vitro* cytotoxicity. *Molecules* 25:819. doi: 10.3390/molecules25040819
- Devi, H. S., Boda, M. A., Shah, M. A., Parveen, S., and Wani, A. H. (2019). Green synthesis of iron oxide nanoparticles using *Platanus orientalis* leaf extract for antifungal activity. *Green Process. Synth.* 8, 38–45. doi: 10.1515/gps-2017-0145

- Du, T., Chen, S., Zhang, J., Li, T., Li, P., Liu, J., et al. (2020). Antibacterial activity of manganese dioxide Nanosheets by ROS-mediated pathways and destroying membrane integrity. *Nanomater* 10:1545. doi: 10.3390/NANO10081545
- Dzul-Erosa, M. S., Cauch-Díaz, M. M., Razo-Lazcano, T. A., Avila-Rodriguez, M., Reyes-Aguilera, J. A., and González-Muñoz, M. P. (2018). Aqueous leaf extracts of *Cnidioscolus chayamansa* (Mayan chaya) cultivated in Yucatán México. Part II: Uses for the phytomediated synthesis of silver nanoparticles. *Mater. Sci. Eng. C* 91, 838–852. doi: 10.1016/j.msec.2018.06.007
- Elbargory, A. M., Hussein, A. A., and Meyer, M. (2019). The *in vitro* immunomodulatory effects of gold nanoparticles synthesized from hypoxis hemerocallidea aqueous extract and hypoxisid on macrophage and natural killer cells. *Int. J. Nanomedicine* 14, 9007–9018. doi: 10.2147/IJN.S216972
- Emam, A. N., Loutfy, S. A., Mostafa, A. A., Awad, H., and Mohamed, M. B. (2017). Cyto-toxicity, biocompatibility and cellular response of carbon dots-plasmonic based nano-hybrids for bioimaging. *RSC Adv.* 7, 23502–23514. doi: 10.1039/c7ra01423f
- Feyzabadi, Z., Ghorbani, F., Vazani, Y., and Zarshenas, M. M. (2017). A critical review on Phytochemistry, Pharmacology of *Viola odorata* L. and Related Multipotential Products in Traditional Persian Medicine. *Phyther. Res.* 31, 1669–1675. doi: 10.1002/ptr.5909
- Gharehyakheh, S., Ahmmeda, A., Haddadi, A., Jamshidi, M., Nowrozi, M., Zangeneh, M. M., et al. (2020). Effect of gold nanoparticles synthesized using the aqueous extract of *Satureja hortensis* leaf on enhancing the shelf life and removing *Escherichia coli* O157:H7 and listeria monocytogenes in minced camel's meat: The role of nanotechnology in the food industry. *Appl. Organomet. Chem.* 34:e5492. doi: 10.1002/aoc.5492
- Gurgur, E., Oluaymo, S. S., Adetuyi, A. O., Omotunde, O. I., and Okoronkwo, A. E. (2020). Green synthesis of zinc oxide nanoparticles and zinc oxide–silver, zinc oxide–copper nanocomposites using *Bridelia ferruginea* as biotemplate. *SN Appl. Sci.* 2, 1–12. doi: 10.1007/s42452-020-2269-3
- Haq, S., Rehman, W., Waseem, M., Shah, A., Khan, A. R., Rehman, M. U., et al. (2020). Green synthesis and characterization of tin dioxide nanoparticles for photocatalytic and antimicrobial studies. *Mater. Res. Express* 7:25012. doi: 10.1088/2053-1591/ab6fa1
- He, Q., Liu, J., Liu, X., Li, G., Chen, D., Deng, P., et al. (2019). A promising sensing platform toward dopamine using MnO<sub>2</sub> nanowires/electro-reduced graphene oxide composites. *Electrochim. Acta* 296, 683–692. doi: 10.1016/j.electacta.2018.11.096
- He, Q., Liu, J., Liu, X., Li, G., Deng, P., and Liang, J. (2018). Manganese dioxide Nanorods/electrochemically reduced graphene oxide nanocomposites modified electrodes for cost-effective and ultrasensitive detection of Amaranth. *Colloids Surfaces B Biointerfaces* 172, 565–572. doi: 10.1016/j.colsurfb.2018.09.005
- Home National Nanotechnology Initiative (2021). Available at: <https://www.nano.gov/> (Accessed June 26, 2021).
- Huang, J., Zhan, G., Zheng, B., Sun, D., Lu, F., Lin, Y., et al. (2011). Biogenic silver nanoparticles by *Cacumen Platycladi* extract: synthesis, formation mechanism, and antibacterial activity. *Ind. Eng. Chem. Res.* 50, 9095–9106. doi: 10.1021/ie200858y
- Iqbal, S., Bhangar, M. I., and Anwar, F. (2005). Antioxidant properties and components of some commercially available varieties of rice bran in Pakistan. *Food Chem.* 93, 265–272. doi: 10.1016/j.foodchem.2004.09.024
- Iqbal, I., and Hamayun, M. (2005). Studies on the traditional uses of plants of Malam Jabba Valley, district swat. *Pakistan. Ethnobot. Leaflet*. 2005:15
- Katoch, M., Singh, A., Singh, G., Wazir, P., and Kumar, R. (2017). Phylogeny, antimicrobial, antioxidant and enzyme-producing potential of fungal endophytes found in *Viola odorata*. *Ann. Microbiol.* 67, 529–540. doi: 10.1007/s13213-017-1283-1
- Khalafi, T., Buazar, F., and Ghanemi, K. (2019). Phycosynthesis and enhanced Photocatalytic activity of zinc oxide nanoparticles Toward Organosulfur pollutants. *Sci. Reports* 9:6866. doi: 10.1038/s41598-019-43368-3
- Khan, S. A., and Lee, C.-S. S. (2020a). “Green Biological Synthesis of Nanoparticles and Their Biomedical Applications” in *Applications of nanotechnology for green synthesis*. eds. Inamuddin, and A. M. Asiri. (Berlin, Germany: Springer Science and Business Media), 247–280.
- Khan, S. A., and Lee, C. S. (2020b). Recent progress and strategies to develop antimicrobial contact lenses and lens cases for different types of microbial keratitis. *Acta Biomater.* 113, 101–118. doi: 10.1016/j.actbio.2020.06.039
- Khan, S. A., Shahid, S., Ayaz, A., Alkahtani, J., Elshikh, M. S., and Riaz, T. (2021a). Phytomolecules-coated NiO nanoparticles synthesis using abutilon indicum leaf extract: antioxidant, antibacterial, and anticancer activities. *Int. J. Nanomedicine* 16, 1757–1773. doi: 10.2147/IJN.S294012
- Khan, S. A., Shahid, S., Hanif, S., Almoallim, H. S., Alharbi, S. A., and Sellami, H. (2021b). Green synthesis of chromium oxide nanoparticles for antibacterial, antioxidant anticancer, and biocompatibility activities. *Int. J. Mol. Sci.* 22:502. doi: 10.3390/ijms22020502
- Khan, S. A., Shahid, S., and Lee, C.-S. S. (2020a). Green synthesis of gold and silver nanoparticles using leaf extract of *Clerodendrum inerme*; characterization, antimicrobial, and antioxidant activities. *Biomol. Ther.* 10:835. doi: 10.3390/biom10060835
- Khan, S. A., Shahid, S., Mahmood, T., and Lee, C.-S. (2021c). Contact lenses coated with hybrid multifunctional ternary nanocoatings (Phytomolecule-coated ZnO nanoparticles:Gallic acid:tobramycin) for the treatment of bacterial and fungal keratitis. *Acta Biomater.* 128, 262–276. doi: 10.1016/j.actbio.2021.04.014
- Khan, S. A., Shahid, S., Shahid, B., Fatima, U., and Abbasi, S. A. (2020b). Green synthesis of MnO nanoparticles using Abutilon indicum leaf extract for biological, Photocatalytic, and adsorption activities. *Biomol. Ther.* 10:785. doi: 10.3390/biom10050785
- Khan, M., Shaik, M. R., Adil, S. F., Khan, S. T., Al-Warthan, A., Siddiqui, M. R. H., et al. (2018). Plant extracts as green reductants for the synthesis of silver nanoparticles: lessons from chemical synthesis. *Dalt. Trans.* 47, 11988–12010. doi: 10.1039/C8DT01152D
- Kim, J. S., Kuk, E., Yu, K. N., Kim, J. H., Park, S. J., Lee, H. J., et al. (2007). Antimicrobial effects of silver nanoparticles. *Nanomedicine nanotechnology. Biol. Med.* 3, 95–101. doi: 10.1016/j.nano.2006.12.001
- Kumar, V., and Yadav, S. K. (2009). Plant-mediated synthesis of silver and gold nanoparticles and their applications. *J. Chem. Technol. Biotechnol.* 84, 151–157. doi: 10.1002/jctb.2023
- Kunkalekar, R. K., Naik, M. M., Dubey, S. K., and Salker, A. V. (2013). Antibacterial activity of silver-doped manganese dioxide nanoparticles on multidrug-resistant bacteria. *J. Chem. Technol. Biotechnol.* 88, 873–877. doi: 10.1002/jctb.3915
- Li, X. Z., and Nikaido, H. (2009). Efflux-mediated drug resistance in bacteria: An update. *Drugs* 69, 1555–1623. doi: 10.2165/11317030-000000000-00000
- López, Y. C., and Antuch, M. (2020). Morphology control in the plant-mediated synthesis of magnetite nanoparticles. *Curr. Opin. Green Sustain. Chem.* 24, 32–37. doi: 10.1016/j.cogsc.2020.02.001
- Manjula, R., Thenmozhi, M., Thilagavathi, S., Srinivasan, R., and Kathirvel, A. (2019). Green synthesis and characterization of manganese oxide nanoparticles from *Gardenia resinifera* leaves. In *Materials Today: Proceedings*; January 7–9, 2019; (Elsevier Ltd.), 3559–3563.
- Muhammad, N., Ur Rehman, N., Khan, H., Saeed, M., and Gilani, A.-H. (2013a). Prokinetic and laxative effects of the crude methanolic extract of *Viola betonicifolia* whole plant in rodents. *BMC Complement. Altern. Med.* 13, 1–7. doi: 10.1186/1472-6882-13-70
- Muhammad, N., Saeed, M., Adhikari, A., Khan, K. M., and Khan, H. (2013b). Isolation of a new bioactive cinnamic acid derivative from the whole plant of *Viola betonicifolia*. *J. Enzyme Inhib. Med. Chem.* 28, 997–1001. doi: 10.3109/14756366.2012.702344
- Muhammad, N., Saeed, M., and Khan, H. (2012). Antipyretic, analgesic and anti-inflammatory activity of *Viola betonicifolia* whole plant. *BMC Complement. Altern. Med.* 12:59. doi: 10.1186/1472-6882-12-59
- Muhammad, N., Saeed, M., Khan, H., and Haq, I. (2013c). Evaluation of n-hexane extract of *Viola betonicifolia* for its neuropharmacological properties. *J. Nat. Med.* 67, 1–8. doi: 10.1007/s11418-012-0636-0
- Muthukumar, T., Sambandam, B., Aravinthan, A., Sastry, T. P., and Kim, J. H. (2016). Green synthesis of gold nanoparticles and their enhanced synergistic antitumor activity using HepG2 and MCF7 cells and their antibacterial effects. *Process Biochem.* 51, 384–391. doi: 10.1016/j.procbio.2015.12.017
- Negahdary, M., Arefian, Z., Dastjerdi, H. A., and Ajdary, M. (2015). Toxic effects of Mn<sub>2</sub>O<sub>3</sub> nanoparticles on rat testis and sex hormone. *J. Nat. Sci. Biol. Med.* 6, 335–339. doi: 10.4103/0976-9668.159998
- New report calls for urgent action to avert antimicrobial resistance crisis (2021). Available at: <https://www.who.int/news/item/29-04-2019-new-report-calls-for-urgent-action-to-avert-antimicrobial-resistance-crisis> (Accessed June 26, 2021).

- Ogunyemi, S. O., Zhang, F., Abdallah, Y., Zhang, M., Wang, Y., Sun, G., et al. (2019). Biosynthesis and characterization of magnesium oxide and manganese dioxide nanoparticles using *Matricaria chamomilla* L. extract and its inhibitory effect on *Acidovorax oryzae* strain RS-2. *Artif. Cells, Nanomed. Biotechnol.* 47, 2230–2239. doi: 10.1080/21691401.2019.1622552
- Panahi-Kalamuei, M., Motevalli, K., and Aliabadi, M. (2016). Rice-like MnO<sub>2</sub> nanoparticles: simple and novel thermal decomposition synthesis, characterization and photocatalytic activity using new precursor. *J. Mater. Sci. Mater. Electron.* 27, 4631–4635. doi: 10.1007/s10854-016-4340-9
- Rafique, M., Sadaf, I., Tahir, M. B., Rafique, M. S., Nabi, G., Iqbal, T., et al. (2019). Novel and facile synthesis of silver nanoparticles using *Albizia procera* leaf extract for dye degradation and antibacterial applications. *Mater. Sci. Eng. C* 99, 1313–1324. doi: 10.1016/j.msec.2019.02.059
- Ramalingam, B., Parandhaman, T., and Das, S. K. (2016). Antibacterial effects of biosynthesized silver nanoparticles on surface ultrastructure and Nanomechanical properties of gram-negative bacteria viz. *Escherichia coli* and *Pseudomonas aeruginosa*. *ACS Appl. Mater. Interfaces* 8, 4963–4976. doi: 10.1021/acsami.6b00161
- Rizwan, K., Khan, S. A., Ahmad, I., Rasool, N., Ibrahim, M., Zubair, M., et al. (2019). A comprehensive review on chemical and pharmacological potential of *Viola betonicifolia*: A plant with multiple benefits. *Molecules* 24:3138. doi: 10.3390/molecules24173138
- Shahid, S., Fatima, U., Shahid, S., Fatima, U., Sajjad, R., and Khan, S. A. (2021). bioinspired nanotheranostic agent: zinc oxide; green synthesis and biomedical potential. *Dig. J. Nanomater. Biostructures* 14, 1023–1031.
- Srither, S. R., Karthik, A., Arunmetha, S., Murugesan, D., and Rajendran, V. (2016). Electrochemical supercapacitor studies of porous MnO<sub>2</sub> nanoparticles in neutral electrolytes. *Mater. Chem. Phys.* 183, 375–382. doi: 10.1016/j.matchemphys.2016.08.041
- Wan, X., Yang, S., Cai, Z., He, Q., Ye, Y., Xia, Y., et al. (2019). Facile synthesis of MnO<sub>2</sub> nanoflowers/N-doped reduced graphene oxide composite and its application for simultaneous determination of dopamine and uric acid. *Nano* 9:847. doi: 10.3390/nano9060847
- Zhu, H., Qin, S. S., Zhang, N., Yang, D. W., Han, H. R., Wei, K. H., et al. (2015). Chemical constituents and biological activities of plants from the genus *Viola*. *Chem. Biodivers.* 12, 1777–1808. doi: 10.1002/cbdv.201400240
- Conflict of Interest:** The authors declare that the research was conducted in the absence of any commercial or financial relationships that could be construed as a potential conflict of interest.
- Publisher's Note:** All claims expressed in this article are solely those of the authors and do not necessarily represent those of their affiliated organizations, or those of the publisher, the editors and the reviewers. Any product that may be evaluated in this article, or claim that may be made by its manufacturer, is not guaranteed or endorsed by the publisher.
- Copyright © 2021 Lu, Zhang, Khan, Li and Wan. This is an open-access article distributed under the terms of the Creative Commons Attribution License (CC BY). The use, distribution or reproduction in other forums is permitted, provided the original author(s) and the copyright owner(s) are credited and that the original publication in this journal is cited, in accordance with accepted academic practice. No use, distribution or reproduction is permitted which does not comply with these terms.